

Floquet-engineered decoherence-resilient protocols for wideband sensing beyond the linear standard quantum limit

Hao Wu,^{1,2,3,*} Clayton Z. C. Ho,^{1,2,3,*} Grant D. Mitts,^{1,2,3,*} Joshua A. Rabinowitz,^{1,2,3} and Eric R. Hudson^{1,2,3}

¹*Department of Physics and Astronomy, University of California Los Angeles, Los Angeles, CA, USA*

²*Challenge Institute for Quantum Computation, University of California Los Angeles, Los Angeles, CA, USA*

³*Center for Quantum Science and Engineering, University of California Los Angeles, Los Angeles, CA, USA*

(Dated: June 4, 2025)

A key advantage of quantum metrology is the ability to surpass the standard quantum limit for measurement precision through the use of non-classical states. However, there is typically little to no improvement in precision with the use of non-classical states for measurements whose duration exceeds the decoherence time of the underlying quantum states. Measurements aimed at the ultimate possible precision are thus performed almost exclusively with classical states and, therefore, are constrained by the standard quantum limit. Here, we demonstrate that by using the phenomenon of subharmonic excitation, in combination with a recently demonstrated technique of Raman excitation of a harmonic oscillator, the frequency of an electric field can be measured at a resolution below the standard quantum limit of the corresponding linear measurement. As the input states can be classical, this metrological gain persists to long timescales and improves the ultimate possible precision. While we demonstrate this technique using motional Raman subharmonic excitation of a single $^{40}\text{Ca}^+$ ion through engineered Floquet states, this technique is expected to be extendable to other platforms, such as NV centers, solid-state qubits, and neutral atoms, where it can provide metrological gain for sensing across the radio frequency, microwave, and optical domains.

Quantum harmonic oscillators (QHOs) serve as highly-sensitive platforms for detecting optical and radio-frequency (RF) electromagnetic fields near the natural frequency ω of the oscillator [1–3]. As a result, QHOs are widely employed as powerful precision sensors in areas such as ultra-precise measurements of force [4–7] and acceleration [8], searches of axionic dark matter [9], and detection of gravitational waves [10]. Importantly, the recent development of a quantum vector signal analyzer (QVSA) based on a single trapped ion has unlocked the potential of QHOs for broadband field sensing by extending the sensing frequency range by nearly three orders of magnitude across the RF and microwave bands [11].

The sensitivity of a QHO-based measurement to a physical parameter θ is bounded by $\sigma_\theta = (\sqrt{F_q(\phi)}(\partial\phi/\partial\theta))^{-1}$, where $F_q(\phi)$ is the Fisher information for a physical quantity ϕ of a QHO in quantum state q . For classical (coherent) states $|\alpha\rangle$, the displacement α is typically a product of the interrogation time τ and a function f that depends on the frequency ω_s and the strength Ω of an applied field (referred to hereafter as the signal field), i.e. $\alpha = \tau f(\omega_s, \Omega)$. Thus, given that the Fisher information for a protocol based on measuring the displacement (α) of the QHO is $F_\alpha \leq 4$, the standard quantum limit (SQL) bounds the sensitivity of the measurement of the signal frequency to $\sigma_{\omega_s} = (2\tau(\partial f/\partial\omega_s))^{-1}$. Further limitations appear in systems with finite coherence time τ_c , where the sensitivity is optimized at $\tau \approx \tau_c/2$ [12].

To further improve sensitivity, non-classical states, such as Schrödinger cat states [1, 13, 14], squeezed states [2, 11], and higher-lying Fock states [3, 15], are employed to surpass the SQL by increasing the Fisher

information to $F_c = 16(|\alpha|^2 + 1/4)$ for cat states, where α is the cat state displacement, $F_s = 4e^{2|r|}$ for squeezed states, where r is the squeezing parameter, and $F_F = 8n + 4$ for fock states, where n is the quanta number, respectively [16]. However, these states are challenging to generate and leverage for sensing, as their coherence times scale inversely with their metrological gain [12]. In practice, extracting gains of 10 dB, for even short timescales, with non-classical states has proven difficult [17].

Here, we introduce the concept of a nonlinear measurement as an alternative means to enhance sensitivity. Specifically, by utilizing the parametric excitation of a QHO subharmonic resonance at frequency $2\omega/K$, where ω is the natural frequency of the QHO and $K \in \mathbb{N}$, in concert with the QVSA technique [11], we demonstrate that the bound on sensitivity for measuring the frequency of a signal field can be improved as much as $\sigma_{\omega_s} = (K\tau(\partial f/\partial\omega_s))^{-1}$ for a Rabi-style measurement; no gain is possible for a Ramsey-style measurement. This $K/2$ enhancement in sensitivity results from the $K/2$ -fold increased dependence of a multiphoton motional Raman process on the frequency of the signal field. Crucially, this gain persists for classical states, meaning that the coherence time, and therefore the limit on τ in a given measurement protocol, does not decrease with K .

In what follows, we describe subharmonic excitation of a QHO and its use as a QVSA to sense a signal field via a multi-photon motional Raman excitation that realizes a QHO displacement with $K/2$ -fold enhanced sensitivity to the signal field frequency. We demonstrate this technique using the motional modes of a single, trapped $^{40}\text{Ca}^+$ ion cooled near its ground state and confirm that the subhar-

monic excitation technique is a nonlinear effect of order K using motional Ramsey spectroscopy. We showcase the wideband nature of the technique by demonstrating field sensing across the RF band with several subharmonic orders, up to $K = 24$, and observe the predicted $2/K$ scaling in sensitivity. Finally, we benchmark the frequency sensitivity of the technique by measuring the Allan deviation for frequency measurements of a signal field as a function of K , finding an improvement by 12.3(9) dB over the corresponding linear SQL. In all cases the SQL for the corresponding linear measurement is surpassed without the use of non-classical QHO states. A minimum frequency uncertainty of 0.56(32) Hz, representing a sixfold improvement over previous measurements [11], is achieved and sets a new bar for the state of the art in QHO-based frequency sensing in the RF regime.

Subharmonic excitation of a harmonic oscillator can be driven by a force oscillating at ω_p whose amplitude depends linearly on the displacement x from equilibrium, i.e. $|\vec{F}| = x(\Omega/2) \cos(\omega_p t)$. The resultant potential $V = x^2 \Omega \cos(\omega_p t)$ can be viewed as a time dependent oscillation of the natural frequency ω of the oscillator, generating a parametric excitation that resonantly excites the oscillator when $\omega_p = 2\omega/K$ for $K \in \mathbb{N}$ [18]. Such excitation leads to a time evolution approximated by a QHO squeezing operator $\hat{S}(r)$ with $r \propto \Omega^K/(\omega/2)^{K-1}$ (see SI Appendix A) and can be viewed as the absorption of K -quanta from the drive field. Subharmonic excitation has been explored in the field of mass spectrometry, where oscillating electric field gradients were used to excite these nonlinear subharmonic resonances to infer the ion mass [19–22]. As this process entails the exchange of K quanta of the driving field for two phonons of the QHO (see Fig. 1 (a)), the resonance condition can be expressed $2\omega = K(\omega_p^{(0)} + \delta)$, where $\omega_p^{(0)} = 2\omega/K$ and δ is the detuning of the drive field from this resonance. As the linewidth of a parametric resonance is a function of the drive field frequency, it also becomes reduced by K – assuming, as discussed later, an appropriate pulse envelope. However, despite the fact that these studies feature linewidths below the corresponding Fourier transform limit (FTL) for the time the driving field was applied, no improvement in mass resolution was observed. This results from the fact that, though the central frequency $\omega_p^{(0)}$ can be determined with K -fold improved sensitivity, i.e. $\partial f/\partial\omega_p \rightarrow K\partial f/\partial\omega_p$, the parametric excitation is no more sensitive to ω , since $\sqrt{F(\omega_p)} = \sqrt{F(\omega)}/K$. Interestingly, though the underlying physical mechanisms are completely different, subharmonic excitation and its concomitant line narrowing have been observed with multiphoton Raman transitions in ultracold atoms [23, 24]; however, again, no useful metrological gain was achieved as the relative frequency of the subharmonic resonance was reduced by the same factor as the line narrowing.

To overcome this sensitivity limitation with subhar-

monic resonances, we employ the QVSA technique [11], which utilizes motional Raman transitions to heterodyne the signal field with an applied probe tone, exciting a subharmonic resonance in the baseband of the QHO. Given the ability to choose the applied probe tone frequency ω_p , this technique allows broadband sensing of ω_s at a sensitivity $K/2$ below the corresponding SQL for a linear measurement.

This method can be understood from the following physical situation. A “signal” tone with voltage V_s and phase ϕ_s at frequency ω_s in a quadrupole configuration (i.e. an electric field with a linear spatial variation) is applied to the ion. In addition, a “probe” tone at frequency $\omega_p = \omega_s + 2\omega_{r/z}/K + \delta$ is applied with a dipole component (i.e. a homogeneous electric field) V_d and a quadrupole component V_q , where $\omega_{r/z}$ is the natural frequency of the QHO on any of the motional modes. The Hamiltonian of the ion motion under these fields is:

$$\begin{aligned} \frac{\hat{H}}{\hbar} &= \omega_{r/z} \hat{a}^\dagger \hat{a} + \Omega_s (\hat{a} + \hat{a}^\dagger)^2 \cos(\omega_s t + \phi_s) \\ &+ \Omega_d (\hat{a} + \hat{a}^\dagger) \cos(\omega_p t) + \Omega_q (\hat{a} + \hat{a}^\dagger)^2 \cos(\omega_p t), \quad (1) \end{aligned}$$

where $\Omega_q = eV_q\eta^2/\hbar$, $\Omega_d = eV_d\eta/\hbar$, $\Omega_s = eV_s\eta^2/\hbar$, and η is the effective Lamb-Dicke parameter. While the dipole tone, Ω_d , is not necessary for the procedure, it is included as given phase mismatch in the system, dipole tones are generally present and consequential as they carry a lower order of η than quadrupole tones. Though careful calibration could eliminate the dipole contribution of the probe tone [11], as seen below, the dipole tone modifies the QVSA process leading to the production of a coherent state, instead of a squeezed state. We find this to be beneficial as coherent states are more easily manipulated. Further, given our readout procedure via a Jaynes-Cummings coupling of the QHO to an optical qubit in a trapped ion, coherent states provide a significantly higher Fisher information than squeezed states (see SI Appendix F).

In the interaction picture with respect to the bare QHO, the Hamiltonian is a sum of eight Hermitian parts each composed of a factor of Ω_i , ladder operators, and a time dependent phase $e^{\pm i\omega_i t}$, where $\{\Omega_1 = \Omega_q, \omega_1 = \omega_p + 2\omega_{r/z}\}$, $\{\Omega_2 = \Omega_q, \omega_2 = \omega_p - 2\omega_{r/z}\}$, $\{\Omega_3 = \Omega_q, \omega_3 = \omega_p\}$, $\{\Omega_4 = \Omega_d, \omega_4 = \omega_p + \omega_{r/z}\}$, $\{\Omega_5 = \Omega_d, \omega_5 = \omega_p - \omega_{r/z}\}$, $\{\Omega_6 = \Omega_s, \omega_6 = \omega_s + 2\omega_{r/z}\}$, $\{\Omega_7 = \Omega_s, \omega_7 = \omega_s - 2\omega_{r/z}\}$, and $\{\Omega_8 = \Omega_s, \omega_8 = \omega_s\}$ (see SI Appendix A).

The dynamics resulting from this Hamiltonian can be analyzed via multimode Floquet theory [25, 26], where the process can be understood as driving virtual motional transitions in a multimode Floquet space. The resulting effective Hamiltonian can be represented as an

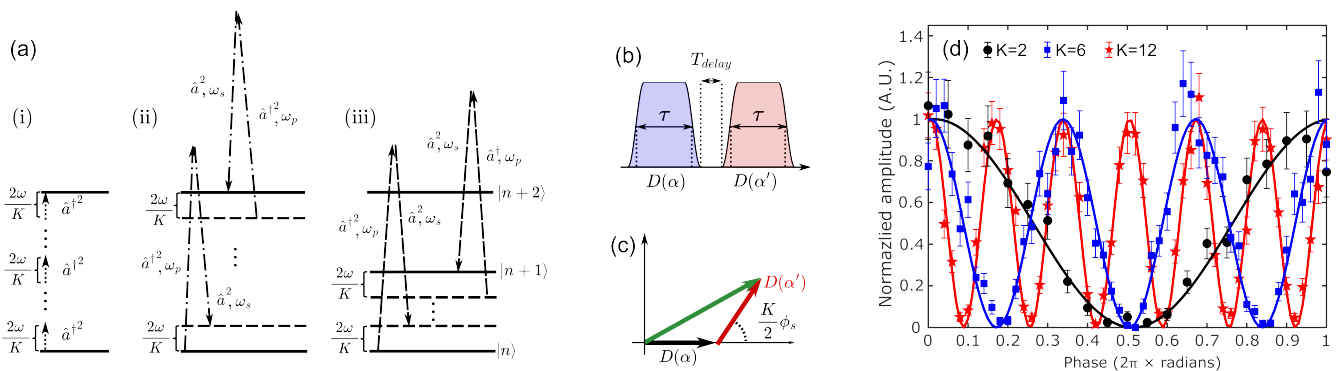


FIG. 1. Energy level diagrams for nonlinear motional excitation and demonstration of K th-order subharmonic Raman excitation via motional Ramsey spectroscopy. (a) Level diagrams for a K th-order parametric excitation (dotted lines), quadrupole subharmonic Raman excitation (dash-dotted lines) and quadrupole/dipole subharmonic Raman excitation (dashed lines). (b-d) Experimental verification of accelerated dynamics via a motional Ramsey sequence with a higher-order subharmonic excitation. (b) Simplified pulse sequence of the motional Ramsey scheme used to examine the phase response. A subharmonic excitation pulse is applied for an interrogation time τ to generate a displacement $\hat{D}(\alpha)$. The ion then evolves freely for some arbitrary delay time. A second identical subharmonic excitation pulse of equal area is then applied with a phase ϕ_s relative to the first pulse to generate a secondary displacement $\hat{D}(\alpha')$, mapping the phase onto the motional state of the ion. (c) Depiction of the motional Ramsey scheme in phase space. Here, the role of the phase ϕ_s can be understood as a rotation of the secondary displacement $\hat{D}(\alpha')$ relative to the first. The phase dependence at order K thus corresponds to the periodicity of the Ramsey fringes. (d) Ramsey fringes generated by scanning the phase ϕ_s of the secondary subharmonic excitation pulse at different orders K . The interrogation time is $\tau = 1$ ms and the delay time is $T_{\text{Delay}} = 50 \mu\text{s}$. Solid lines are fits of the data to a sine function. The motional excitation amplitudes for each subharmonic order K are normalized for comparison. Error bars represent one standard error.

eight-mode Floquet Hamiltonian [25, 26]:

$$\hat{H} = \sum_{K=1}^{\infty} \sum_{i=1}^8 \left(\hat{H}_1^{(i)} + \hat{H}_2^{(i)} + \dots + \hat{H}_K^{(i)} \dots \right) \times e^{-i(\sum_{k=1}^8 c_k \omega_k)t} e^{-i(c_6 + c_7 + c_8)\phi_s} \quad (2)$$

While lower-order terms can be readily obtained using the methods outlined in Refs. [25, 26], deriving a general analytical expression for the K th-order perturbation term $\hat{H}_K^{(i)}$ is nontrivial. Nonetheless, the basic principles are apparent from Eqn. (2). A resonant displacement results when the condition $\sum_k c_k \omega_k = 0$ is satisfied. Since $c_k \in \mathbb{Z}$, this constraint leads to the restrictions: for the probe tones $\sum_{k=1}^5 c_k = \pm K/2$ and for the signal tone $\sum_{k=6}^8 c_k = \mp K/2$.

This result has several consequences. First, it is clear that the detuning δ is amplified by a factor of $\sum_{k=1}^5 c_k = K/2$, narrowing the linewidth relative to a linear measurement by up to $2/K$. Second, the K th-order Hamiltonian $H_K^{(i)}$ involves $K-1$ commutation operations [25, 26]. Since all Fourier components $H_K^{(i)}$ are comprised of only first-order (\hat{a}, \hat{a}^\dagger) or second-order ($\hat{a}^2, \hat{a}^{\dagger 2}, \hat{a}^\dagger \hat{a}$) ladder operators, the commutators of the K th-order Hamiltonian are nonvanishing only when the number of first-order ladder operators is exactly one; this occurs if the dipole tone contributes only one of K terms in the Hamiltonian (see SI Appendix B). These criteria determine the number of tones needed at each frequency, such that the displace-

ment α scales as

$$\alpha = \beta(\omega_s, K, \omega_{r/z}) \Omega_d \Omega_q^{(K-2)/2} \Omega_s^{K/2} e^{-i\phi_s K/2}, \quad (3)$$

where β is a function of the signal frequency ω_s , the oscillator frequency $\omega_{r/z}$, and the subharmonic order K (see SI Appendix B). Near $\delta = 0$, $\partial\beta/\partial\delta \propto K/2$. The multi-mode Floquet process can be illustrated as multiphoton transitions, as shown in Fig. 1(a). The dash-dotted line represents the subharmonic excitation for a quadrupole-only configuration (ii), while the dashed lines indicate excitation for a quadrupole/dipole configuration (iii).

To verify this result and demonstrate the technique, we realize a QHO using a single trapped $^{40}\text{Ca}^+$ ion with a radial (axial) secular frequency $\omega_r \approx 2\pi \cdot 1$ MHz ($\omega_z \approx 2\pi \cdot 0.7$ MHz). Doppler cooling of the ion followed by resolved-sideband cooling on the optical qubit transition prepares the motional ground state of the radial (axial) mode with $\langle n \rangle \approx 0.01(1)$ ($\langle n \rangle \approx 0.01(1)$). The dephasing time τ_c of the radial (axial) mode without applying external fields is ≈ 2 ms (≈ 20 ms). The mean phonon number $\langle n \rangle$ is measured using either blue sideband (BSB) Rabi oscillations [27] or sideband ratio comparison [11].

Subharmonic excitation can be driven on any of the QHO modes by applying to the trap electrodes both the signal tone voltage at frequency ω_s in a quadrupole configuration and the probe tone voltage at a frequency $\omega_p = \omega_s + 2\omega/K + \delta$ with both dipole and quadrupole components (see SI Appendix A). In what follows, we

assume that any AC stark shifts of the QHO frequency generated by the quadrupole tones have been absorbed into the resonance condition. Pulses are applied with a tapered-cosine envelope to mitigate off-resonant motional excitation [28].

First, it is important to verify that the displacement induced by the subharmonic excitation arises from a K th-order perturbation following Eqn. 3. While this could be assessed by measuring the phonon number as a function of applied voltage, the limited dynamic range of our readout technique makes it challenging to accurately characterize the sharp power law growth expected at higher orders. Therefore, we employ a motional Ramsey sequence [3], depicted in Fig. 1(b). Following cooling near the motional ground state $|0\rangle$, a resonant subharmonic excitation pulse is applied for some interrogation time τ to generate a displacement $\hat{D}(\alpha)$. The ion is then allowed to freely evolve for some delay time T_{Delay} , after which a second resonant subharmonic excitation with equal pulse area but relative phase ϕ_s is applied to generate a secondary displacement $\hat{D}(\alpha')$. For a K th-order process, this leads to a phase shift $K\phi_s/2$ of the displacement, as confirmed in Fig. 1(d) for $K=2, 6$, and 12. Further, the resulting motional state was examined via the BSB Rabi oscillation method and found to be a coherent state, as expected (see insets in Fig. 2 (a, b)).

To demonstrate the technique's ability to reduce the linewidth below the corresponding linear SQL, the frequency of a signal tone was measured by sweeping the frequency of the probe tone across the subharmonic resonance for several different orders, as shown in Fig. 2 (a, b) for the radial and axial modes, respectively. The resultant motional state was measured via the sideband ratio method. Linewidths were extracted by fitting a sinc-squared profile $|\beta(\omega_p)|^2$ to the data (plotted in Fig. 2 (c)). For $K \geq 4$, the spectral linewidth of the subharmonic surpasses the corresponding linear SQL, shown as dashed lines in Fig. 2 (c), with a minimum linewidth $\approx 6\times$ narrower than the corresponding linear SQL for $K = 12$. To demonstrate arbitrary frequency operation below the corresponding linear SQL, we excite the $K = 6$ subharmonic at $\omega_s/2\pi = 70, 80$ and 200 MHz and recover highly overlapped lineshapes (see SI Appendix D).

As seen in Fig. 2 (c), the measured linewidths narrow approximately as $2/K$. The $2/K$ line is the maximum achievable narrowing and is only achieved for a 'square wave' interaction envelope. For non-square pulse envelopes, such as Blackman or Gaussian envelopes, the nonlinear interaction results in a reduced evolution time, or equivalently, the nonlinear pulse exhibits a broader spectral width, reducing the narrowing effect. As a compromise between the off-resonant excitation of the square envelope and the desire to retain the narrowing effect, we use a tapered-cosine pulse as shown in Fig. 1(b).

Next, we study the ability of the technique to provide useful metrological gain relative to the correspond-

ing linear SQL. Here, the motional lineshape of a subharmonic excitation is first measured, as shown in Fig. 2 (a, b). Subsequent frequency measurements are then conducted by measuring the two points at the full-width at half maximum, where sensitivity is balanced with intrinsic noise, and fitting the result to determine the center frequency. Finally, the overlapping Allan deviations are computed from this data and shown in Figs. 3 (a, b) for an 80 MHz signal tone at various subharmonic orders K on the radial and axial modes, respectively. For comparison, the solid line represents the corresponding linear SQL, computed from the given pulse area. A minimum frequency resolution of 0.85(18) Hz was achieved after $N \approx 16000$ experiments using the $K = 12$ order subharmonic on the axial mode. The maximum metrological gain of $20\log_{10}(\sigma_{\text{SQL}}/\sigma_{\omega_s})=12.3(9)$ dB over the linear SQL was realized at $N \approx 1600$ with interrogation time $\tau = 2$ ms. Likewise, a gain of 4.9(8) dB was obtained on the radial mode with $K = 24$, achieving a minimum resolution of 2.3(2) Hz after $N \approx 7200$ experiments with interrogation time $\tau = 2$ ms. The reduction in performance of measurements on the radial mode is due to a combination of increased off-resonant motional excitation and larger radial secular frequency instability. The maximum achievable orders are limited to $K = 24$ for the radial mode and $K = 12$ for the axial mode by the requisite higher power levels required for higher order operation, which induces faster motional decoherence. These effects can be mitigated by enhancing the RF coupling efficiency, thereby reducing the required input power.

The achieved 12.3(9) dB gain is comparable to that expected using a linear measurement with a nonclassical, $|n \approx 20\rangle$ Fock state [29]. However, there is one crucial difference. Non-classical states, such as Fock states and cat states, achieve enhanced sensitivity in parameter estimation by increasing the separation between superposed states in the system state vector. As expected from quantum speedlimit theorems [30], greater separation results in larger phase accumulation, leading to improved Fisher information. However, the coherence time of Fock states typically goes as $1/n^p$ with $p \geq 1$, reducing the useful measurement time for these states [31, 32]. As a result, non-classical states typically do not provide any metrological gain over the SQL for the ultimate precision of a frequency measurement. Because our nonlinear measurement uses a classical input state, it avoids the coherence time limitations typically associated with non-classical states, allowing metrological gain to be realized in the ultimate precision of a frequency measurement.

Finally, by applying a pulse with interrogation time $\tau = 5$ ms on the axial mode, a minimum frequency uncertainty $\delta\omega_s/2\pi = 0.56(32)$ Hz at 80 MHz was achieved (see SI Appendix E). To our knowledge, this sets the state of the art for frequency sensing on a QHO in the radio-frequency band. This measurement could easily be improved by a factor of $4\times$ by improving the dam-

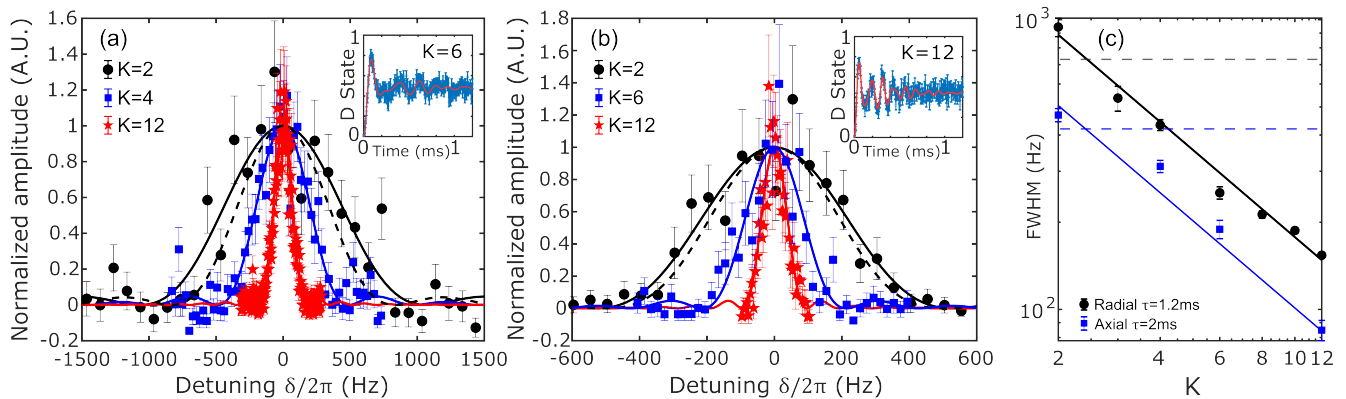


FIG. 2. Demonstration of linewidth narrowing exceeding the linear standard quantum limit (SQL) using subharmonic excitation. (a, b) Application of subharmonic excitation towards sensing of an “unknown” signal at $\omega_s/2\pi = 70$ MHz on the radial mode (a) and $\omega_s/2\pi = 80$ MHz on the axial mode (b). The frequency of the “unknown” tone is determined by scanning the frequency of the probe tones and maximizing the signal amplitude. To aid visual comparison, measured phonon numbers are normalized by the amplitudes of the corresponding fits to give a “normalized amplitude.” Solid lines are fits of the data to a sinc-squared lineshape. Insets in (a) and (b): Blue sideband (BSB) Rabi oscillations characterize the motional state after subharmonic excitation. Solid red lines are fits assuming a motional coherent state. (c) Characterization of the dependence of linewidth on the subharmonic order K . The linewidth is defined as the Full-Width at Half Maximum (FWHM). The solid line is a linear fit to the data with no offset. (a, black data in c) The effective interrogation time is fixed at $\tau = 1.2$ ms for different values of K . (b, blue data in c) The effective interrogation time is fixed at $\tau = 2.0$ ms for different values of K . The effective interrogation time τ is given as the pulse width of a square pulse of equivalent amplitude and area. (a, b, c) The dashed lines indicate the Fourier transform limit (FTL) of the applied tapered-cosine pulse envelope, and corresponds to linear SQL. $\omega_{r/z}$ is the secular frequency of the radial (axial) mode. Error bars represent one standard error.

age threshold of system electronics, with further gains achievable by extending the motional coherence times to allow longer interrogation periods.

In summary, we have demonstrated that by utilizing Floquet-engineered motional Raman subharmonic excitation, high-resolution frequency measurements can be achieved below the corresponding linear standard quantum limit. This technique is adaptable to other platforms, including nitrogen-vacancy centers, superconducting circuits, and neutral atom systems, where Raman transitions can be driven between two energy levels. Thus, with a stable reference, this method allows for the measurement of electromagnetic field frequencies across the RF, microwave, and even optical domains. This protocol is compatible with the use of nonclassical motional states, such as Fock states [3, 15, 29, 33], which could further improve precision for measurements at short timescales. Finally, because the technique can be used with classical input states, it does not suffer from the reduction in coherence time that limits measurements using nonclassical states. Therefore, the metrological gain demonstrated here provides improvement of the ultimate precision possible in a frequency measurement.

ACKNOWLEDGEMENTS

We thank Dylan Kawashiri for building a computer cluster used to simulate these results. This work was

supported by NSF (PHY-2110421 and OMA-2016245), AFOSR (130427-5114546), and ARO (W911NF-19-1-0297).

COMPETING INTERESTS

The authors declare no competing interests.

-
- * These authors contributed equally to this work
- [1] C. Hempel, B. P. Lanyon, P. Jurcevic, R. Gerritsma, R. Blatt, and C. F. Roos, Entanglement-enhanced detection of single-photon scattering events, *Nature Photonics* **7**, 630 (2013).
 - [2] S. C. Burd, R. Srinivas, J. J. Bollinger, A. C. Wilson, D. J. Wineland, D. Leibfried, D. H. Slichter, and D. T. C. Allcock, Quantum amplification of mechanical oscillator motion, *Science* **364**, 1163 (2019), doi: 10.1126/science.aaw2884.
 - [3] F. Wolf, C. Shi, J. C. Heip, M. Gessner, L. Pezzè, A. Smerzi, M. Schulte, K. Hammerer, and P. O. Schmidt, Motional fock states for quantum-enhanced amplitude and phase measurements with trapped ions, *Nature Communications* **10**, 2929 (2019).
 - [4] S. Knünz, M. Herrmann, V. Batteiger, G. Saathoff, T. W. Hänsch, K. Vahala, and T. Udem, Injection locking of a trapped-ion phonon laser, *Phys. Rev. Lett.* **105**, 013004 (2010).

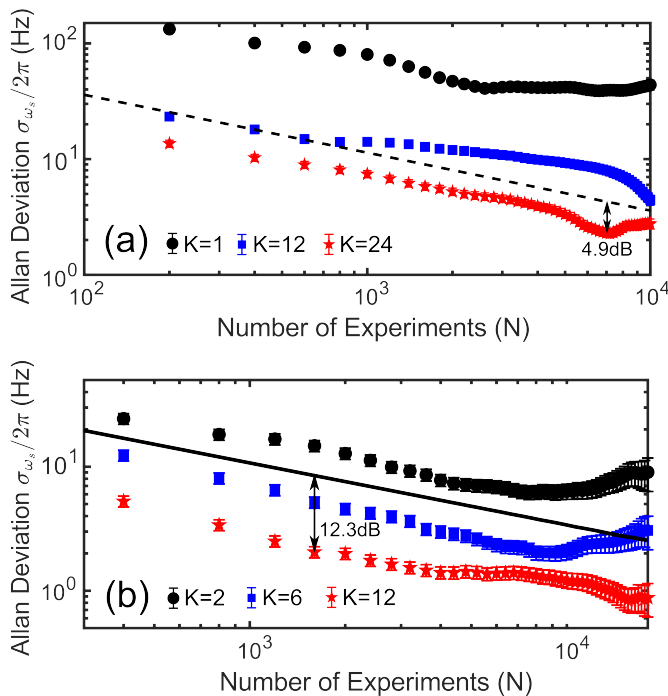


FIG. 3. Frequency sensitivity of the subharmonic protocol. (a-b) Overlapping Allan deviations of frequency for an 80 MHz tone at different subharmonic orders K on the radial (a) and axial (b) modes. Each experiment takes ~ 17 ms. Solid lines represent the corresponding SQL for the given interrogation time, which corresponds with the SQL of the $K = 2$ subharmonic excitation. (a) Subharmonic excitation is probed on the radial mode with an interrogation time of $\tau = 2$ ms. A minimum frequency resolution $\delta\omega_s/2\pi = 2.3(2)$ Hz is achieved using the $K = 24$ order after $N \approx 7200$ experiments. A maximum metrological gain of 4.9(8) dB is similarly achieved using the $K = 24$ order after $N \approx 7000$ experiments. (b) Subharmonic excitation is probed on the axial mode with an interrogation time of $\tau = 2$ ms. A minimum frequency resolution $\delta\omega_s/2\pi = 0.85(18)$ Hz is achieved using the $K = 12$ order after $N \approx 16000$ experiments. A maximum metrological gain of 12.3(9) dB is achieved using the same $K = 12$ order after $N \approx 1600$ experiments. Error bars represent one standard error.

[5] M. J. Biercuk, H. Uys, J. W. Britton, A. P. VanDevender, and J. J. Bollinger, Ultrasensitive detection of force and displacement using trapped ions, *Nature Nanotechnology* **5**, 646 (2010).
 [6] K. A. Gilmore, J. G. Bohnet, B. C. Sawyer, J. W. Britton, and J. J. Bollinger, Amplitude sensing below the zero-point fluctuations with a two-dimensional trapped-ion mechanical oscillator, *Phys. Rev. Lett.* **118**, 263602 (2017).
 [7] Z. Liu, Y. Wei, L. Chen, J. Li, S. Dai, F. Zhou, and M. Feng, Phonon-laser ultrasensitive force sensor, *Phys. Rev. Appl.* **16**, 044007 (2021).
 [8] W. C. Campbell and P. Hamilton, Rotation sensing with trapped ions*, *Journal of Physics B: Atomic, Molecular and Optical Physics* **50**, 064002 (2017).

[9] R. Bradley, J. Clarke, D. Kinion, L. J. Rosenberg, K. van Bibber, S. Matsuki, M. Mück, and P. Sikivie, Microwave cavity searches for dark-matter axions, *Rev. Mod. Phys.* **75**, 777 (2003).
 [10] B. P. Abbott *et al.* (LIGO Scientific Collaboration and Virgo Collaboration), Observation of gravitational waves from a binary black hole merger, *Phys. Rev. Lett.* **116**, 061102 (2016).
 [11] H. Wu, G. D. Mitts, C. Z. C. Ho, J. A. Rabinowitz, and E. R. Hudson, Wideband electric field quantum sensing via motional raman transitions, *Nature Physics* **10.1038/s41567-024-02753-0** (2025).
 [12] S. F. Huelga, C. Macchiavello, T. Pellizzari, A. K. Ekert, M. B. Plenio, and J. I. Cirac, Improvement of frequency standards with quantum entanglement, *Phys. Rev. Lett.* **79**, 3865 (1997).
 [13] K. G. Johnson, J. D. Wong-Campos, B. Neyenhuis, J. Mizrahi, and C. Monroe, Ultrafast creation of large schrödinger cat states of an atom, *Nature Communications* **8**, 697 (2017).
 [14] C. Monroe, D. M. Meekhof, B. E. King, and D. J. Wineland, A “schrödinger cat” superposition state of an atom, *Science* **272**, 1131 (1996).
 [15] K. C. McCormick, J. Keller, S. C. Burd, D. J. Wineland, A. C. Wilson, and D. Leibfried, Quantum-enhanced sensing of a single-ion mechanical oscillator, *Nature* **572**, 86 (2019).
 [16] F. Wolf, *Motional quantum state engineering for quantum logic spectroscopy of molecular ions*, Ph.D. thesis, Leibniz Universität at Hannover (2018).
 [17] L. Pezzè, A. Smerzi, M. K. Oberthaler, R. Schmied, and P. Treutlein, Quantum metrology with nonclassical states of atomic ensembles, *Rev. Mod. Phys.* **90**, 035005 (2018).
 [18] L. D. Landau and E. M. Lifshitz, *Mechanics, Third Edition: Volume 1 (Course of Theoretical Physics)*, 3rd ed. (Butterworth-Heinemann, 1976).
 [19] M. Sudakov, N. Kononov, D. Douglas, and T. Glebova, Excitation frequencies of ions confined in a quadrupole field with quadrupole excitation, *Journal of the American Society for Mass Spectrometry* **11**, 10 (2000).
 [20] X. Zhao, V. L. Ryjkov, and H. A. Schuessler, Parametric excitations of trapped ions in a linear rf ion trap, *Phys. Rev. A* **66**, 063414 (2002).
 [21] B. Collings and D. Douglas, Observation of higher order quadrupole excitation frequencies in a linear ion trap, *Journal of the American Society for Mass Spectrometry* **11**, 1016 (2000).
 [22] G. Tammaseo, P. Paasche, C. Angelescu, and G. Werth, Subharmonic excitation of the eigenmodes of charged particles in a penning trap, *Eur. Phys. J. D* **28**, 39 (2003).
 [23] R. Trebino and L. A. Rahn, Subharmonic resonances in higher-order collision-enhanced wave mixing in a sodium-seeded flame, *Opt. Lett.* **12**, 912 (1987).
 [24] F. S. Cataliotti, R. Scheunemann, T. W. Hänsch, and M. Weitz, Superresolution of pulsed multiphoton raman transitions, *Phys. Rev. Lett.* **87**, 113601 (2001).
 [25] M. Ernst, A. Samoson, and B. H. Meier, Decoupling and recoupling using continuous-wave irradiation in magic-angle-spinning solid-state nmr: A unified description using bimodal floquet theory, *The Journal of Chemical Physics* **123**, 064102 (2005), https://pubs.aip.org/aip/jcp/article-pdf/doi/10.1063/1.1944291/15368777/064102_1.online.pdf.

- [26] G. Wang, Y.-X. Liu, J. M. Schloss, S. T. Alsid, D. A. Braje, and P. Cappellaro, Sensing of arbitrary-frequency fields using a quantum mixer, *Phys. Rev. X* **12**, 021061 (2022).
- [27] D. Leibfried, R. Blatt, C. Monroe, and D. Wineland, Quantum dynamics of single trapped ions, *Rev. Mod. Phys.* **75**, 281 (2003).
- [28] G. Zarantonello, H. Hahn, J. Morgner, M. Schulte, A. Bautista-Salvador, R. F. Werner, K. Hammerer, and C. Ospelkaus, Robust and resource-efficient microwave near-field entangling $^9\text{Be}^+$ gate, *Phys. Rev. Lett.* **123**, 260503 (2019).
- [29] X. Deng, S. Li, Z.-J. Chen, Z. Ni, Y. Cai, J. Mai, L. Zhang, P. Zheng, H. Yu, C.-L. Zou, S. Liu, F. Yan, Y. Xu, and D. Yu, Quantum-enhanced metrology with large fock states, *Nature Physics* [10.1038/s41567-024-02619-5](https://doi.org/10.1038/s41567-024-02619-5) (2024).
- [30] S. Deffner and S. Campbell, Quantum speed limits: from heisenberg's uncertainty principle to optimal quantum control, *Journal of Physics A: Mathematical and Theoretical* **50**, 453001 (2017).
- [31] Q. A. Turchette, C. J. Myatt, B. E. King, C. A. Sackett, D. Kielpinski, W. M. Itano, C. Monroe, and D. J. Wineland, Decoherence and decay of motional quantum states of a trapped atom coupled to engineered reservoirs, *Phys. Rev. A* **62**, 053807 (2000).
- [32] C. J. Myatt, B. E. King, Q. A. Turchette, C. A. Sackett, D. Kielpinski, W. M. Itano, C. Monroe, and D. J. Wineland, Decoherence of quantum superpositions through coupling to engineered reservoirs, *Nature* **403**, 269 (2000).
- [33] F. Wolf and P. Schmidt, Quantum sensing of oscillating electric fields with trapped ions, *Measurement: Sensors* **18**, 100271 (2021).
- [34] J. Johansson, P. Nation, and F. Nori, Qutip: An open-source python framework for the dynamics of open quantum systems, *Computer Physics Communications* **183**, 1760 (2012).
- [35] J. Johansson, P. Nation, and F. Nori, Qutip 2: A python framework for the dynamics of open quantum systems, *Computer Physics Communications* **184**, 1234 (2013).

Supplementary Information

Appendix A: Theoretical Analysis

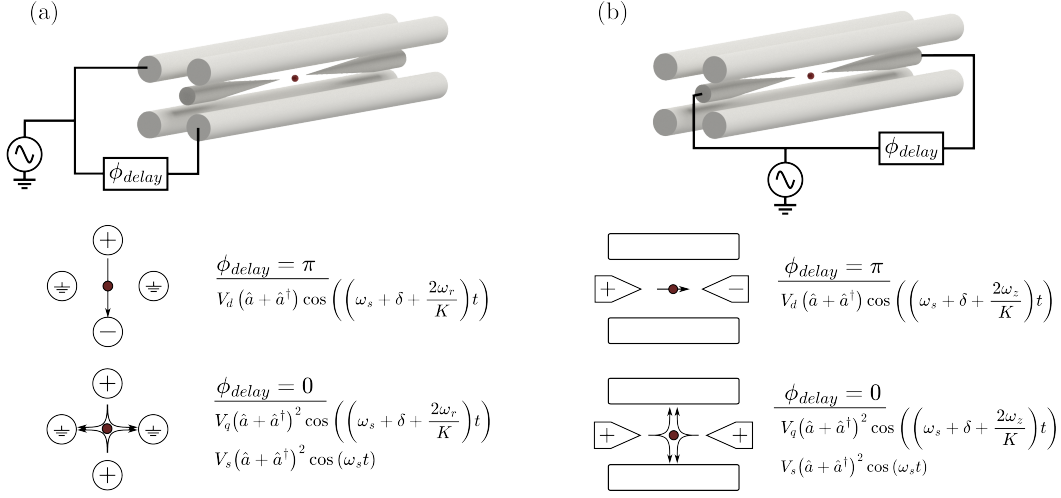


FIG. 4. Implementation of subharmonic excitation on the radial and axial modes, respectively. (a) Subharmonic excitation is applied to excite the radial motional mode by coupling an oscillating voltage onto a pair of opposing trap electrodes. (b) The axial motional mode can be excited by instead coupling the voltage onto the axial endcaps of the trap. A dipole field is generated for a relative phase $\phi_{delay} = \pi$ between the voltages coupled to the electrodes, while a quadrupole field is generated if the coupled voltages are exactly in phase (i.e. $\phi_{delay} = 0$).

In this section, we derive the dynamics of motional excitation on a subharmonic resonance within the framework of multimode Floquet theory [25, 26]. Consider an unknown signal tone ω_s to be detected, which is coupled to the trapping electrodes in a quadrupole configuration. Additionally, a probe tone ω_p is applied in a combination of dipole and quadrupole configurations as shown in Fig. 4. The resulting Hamiltonian representing the motional state of the harmonic oscillator and electric field coupling can be is:

$$\begin{aligned} \frac{\hat{H}}{\hbar} = & \omega_{r/z} \hat{a}^\dagger \hat{a} + \Omega_q (\hat{a} + \hat{a}^\dagger)^2 \cos(\omega_p t) \\ & + \Omega_d (\hat{a} + \hat{a}^\dagger) \cos(\omega_p t) \\ & + \Omega_s (\hat{a} + \hat{a}^\dagger)^2 \cos(\omega_s t + \phi_s), \end{aligned} \quad (4)$$

where $\omega_p = \omega_s + \delta + 2\omega_{r/z}/K$, $\Omega_q = eV_q \eta^2 / \hbar$, $\Omega_d = eV_d \eta / \hbar$, $\Omega_s = eV_s \eta^2 / \hbar$, $\eta = x_0 / r_0$ is effective Lamb-Dicke parameter, r_0 is the ion-electrode distance, $x_0 = \sqrt{\hbar / (2m\omega_{r/z})}$ is the zero-point wavefunction of the QHO, e is the electron charge, and δ is the detuning. Without loss of generality, we ignore the phase of the probe tones and use ω to represent $\omega_{r/z}$.

Unlike previous schemes [19–22] which have exclusively employed quadrupole tones, the present approach applies an additional probe tone in the dipole configuration for several reasons:

- The effective Lamb-Dicke parameter η associated with a dipole tone is of a lower order than that of quadrupole tones, which reduces the power threshold required to excite higher-order subharmonics.
- Application of a dipole tone induces motional excitation that generates a coherent state rather than a squeezed state. Coherent states operate within a linear regime compared to squeezed states, making them more straightforward to manipulate compared to a squeezed state.
- Measurement of a coherent state provides higher Fisher information, leading to enhanced sensitivity in parameter estimation, such as for frequency measurements.

Transforming into the interaction picture with respect to $\omega\hat{a}^\dagger\hat{a}$, the Hamiltonian (4) becomes:

$$\begin{aligned}
\frac{\hat{H}_I}{\hbar} = & +\Omega_q/2 \left(\hat{a}^2 e^{-i(2\omega+\omega_p)t} + \hat{a}^{\dagger 2} e^{i(2\omega+\omega_p)t} \right) \\
& +\Omega_q/2 \left(\hat{a}^2 e^{i(\omega_p-2\omega)t} + \hat{a}^{\dagger 2} e^{-i(\omega_p-2\omega)t} \right) \\
& +\Omega_q/2 \left(2\hat{a}^\dagger\hat{a} + 1 \right) \left(e^{i\omega_p t} + e^{-i\omega_p t} \right) \\
& +\Omega_d/2 \left(\hat{a} e^{-i(\omega+\omega_p)t} + \hat{a}^\dagger e^{i(\omega+\omega_p)t} \right) \\
& +\Omega_d/2 \left(\hat{a} e^{i(\omega_p-\omega)t} + \hat{a}^\dagger e^{-i(\omega_p-\omega)t} \right) \\
& +\Omega_s/2 \left(\hat{a}^2 e^{-i(2\omega+\omega_s+\phi_s)t} + (\hat{a}^\dagger)^2 e^{i(2\omega+\omega_s+\phi_s)t} \right) \\
& +\Omega_s/2 \left(\hat{a}^2 e^{i(\omega_s-2\omega+\phi_s)t} + \hat{a}^{\dagger 2} e^{-i(\omega_s-2\omega+\phi_s)t} \right) \\
& +\Omega_s/2 \left(2\hat{a}^\dagger\hat{a} + 1 \right) \left(e^{i(\omega_s t+\phi_s)} + e^{-i(\omega_s t+\phi_s)} \right)
\end{aligned} \tag{5}$$

Within the framework of multimode Floquet theory [25, 26], the effective Hamiltonian \hat{H}_I can be represented as an eight-mode Floquet Hamiltonian:

$$\begin{aligned}
\bar{H}_I(t) = & \sum_{\langle c_1, c_2, c_3, c_4, c_5, c_6, c_7, c_8 \rangle} \left(H_{(1)}^{(c_1, c_2, c_3, c_4, c_5, c_6, c_7, c_8)} + H_{(2)}^{(c_1, c_2, c_3, c_4, c_5, c_6, c_7, c_8)} + \dots + H_{(K)}^{(c_1, c_2, c_3, c_4, c_5, c_6, c_7, c_8)} + \dots \right) \\
& \cdot e^{-i(\sum_{k=1}^8 c_k \omega_k)t - i(c_6+c_7+c_8)\phi_s},
\end{aligned} \tag{6}$$

where for $H_{(K)}^{(c_1, c_2, c_3, c_4, c_5, c_6, c_7, c_8)}$, the subscript K denotes the corresponding order of subharmonic excitation and the number of tones involved in the nonlinear process, while the superscript values $(c_1, c_2, c_3, c_4, c_5, c_6, c_7, c_8)$ represent the eight selectable tones – $\omega_1 = \omega_p + 2\omega$, $\omega_2 = \omega_p - 2\omega$, $\omega_3 = \omega_p$, $\omega_4 = \omega_p + \omega$, $\omega_5 = \omega_p - \omega$, $\omega_6 = \omega_s + 2\omega$, $\omega_7 = \omega_s - 2\omega$, and $\omega_8 = \omega_s$.

The Fourier components corresponding to the eight selectable tones are given as follows:

$$\begin{aligned}
H^{(0,-1,0,0,0,0,0,0)} & = H^{(1,0,0,0,0,0,0,0)} = \Omega_q/2(\hat{a}^\dagger)^2, \\
H^{(0,1,0,0,0,0,0,0)} & = H^{(-1,0,0,0,0,0,0,0)} = \Omega_q/2(\hat{a})^2, \\
H^{(0,0,-1,0,0,0,0,0)} & = H^{(0,0,1,0,0,0,0,0)} = \Omega_q/2(2\hat{a}^\dagger\hat{a} + 1), \\
H^{(0,0,0,0,-1,0,0,0)} & = H^{(0,0,0,1,0,0,0,0)} = \Omega_d/2(\hat{a}^\dagger), \\
H^{(0,0,0,0,1,0,0,0)} & = H^{(0,0,0,-1,0,0,0,0)} = \Omega_d/2(\hat{a}), \\
H^{(0,0,0,0,0,-1,0)} & = H^{(0,0,0,0,0,1,0,0)} = \Omega_s/2(\hat{a}^\dagger)^2, \\
H^{(0,0,0,0,0,0,1,0)} & = H^{(0,0,0,0,0,-1,0,0)} = \Omega_s/2(\hat{a})^2, \\
H^{(0,0,0,0,0,0,0,-1)} & = H^{(0,0,0,0,0,0,0,1)} = \Omega_s/2(2\hat{a}^\dagger\hat{a} + 1),
\end{aligned} \tag{7}$$

When the resonance condition $\sum_{k=1}^8 c_k \omega_k = 0$ is satisfied, a higher-order subharmonic is excited, generating a motional displacement. The resonance condition can be reduced to $(\sum_{k=1}^8 c_k)\omega_s + ((\sum_{k=1}^5 c_k)2/K + (2c_1 - 2c_2 + c_4 - c_5 + 2c_6 - 2c_7))\omega + (\sum_{k=1}^5 c_k)\delta = 0$ to yield the constraints:

$$\begin{aligned}
c_1 + c_2 + c_3 + c_4 + c_5 + c_6 + c_7 + c_8 & = 0, \\
(2c_1 - 2c_2 + c_4 - c_5 + 2c_6 - 2c_7) & = -1, \\
c_1 + c_2 + c_3 + c_4 + c_5 & = K/2.
\end{aligned} \tag{8}$$

These constraints can be intuitively understood as a multi-phonon Raman transition. To generate a displacement resonant with the secular frequency ω , the number of probe tones must match the number of signal tones to cancel the carrier frequency ω_s .

Creating a general analytical expression for an arbitrary K th-order Hamiltonian that includes all parameters is nontrivial. Instead, we here derive an empirical formula.

The K th-order Hamiltonian $H_{(K)}^{(c_1, c_2, c_3, c_4, c_5, c_6, c_7, c_8)}$ involves $K-1$ commutation operations [25, 26]. From (7), all Fourier components $H_{(K)}^{(c_1, c_2, c_3, c_4, c_5, c_6, c_7, c_8)}$ are comprised of only first-order (\hat{a} , \hat{a}^\dagger) or second-order (\hat{a}^2 , $\hat{a}^{\dagger 2}$, $\hat{a}^\dagger \hat{a}$) ladder operators. The commutation between ladder operators is nonvanishing only when the number of first-order ladder operators is exactly one, which occurs only if the dipole tone contributes only one of K terms in the Hamiltonian. Together with the resonance constraints, we arrive at an empirical formula for subharmonic driving of a coherent state:

$$\alpha = \beta(\omega_s, K, \omega) \Omega_d \Omega_q^{(K-2)/2} \Omega_s^{K/2} e^{-i\phi_s K/2}, \quad (9)$$

where β is a function of the signal frequency ω_s , the secular frequency ω , and the subharmonic order K , and can be numerically calculated from QuTip simulations [34, 35].

To validate the Floquet theory for the subharmonic excitation, we consider the case of $K=2$ as an example. The second-order term for eight-mode Floquet theory can be expressed as:

$$H_{(2)}^{(c_1, c_2, c_3, c_4, c_5, c_6, c_7, c_8)} = -\frac{1}{2} \sum_{\substack{c'_1, c'_2, c'_3, c'_4, \\ c'_5, c'_6, c'_7, c'_8}} \frac{[H_{(2)}^{(c_1, c_2, c_3, c_4, c_5, c_6, c_7, c_8)}, H_{(2)}^{(c'_1 - c_1, c'_2 - c_2, c'_3 - c_3, c'_4 - c_4, c'_5 - c_5, c'_6 - c_6, c'_7 - c_7, c'_8 - c_8)}]}{\sum_{k=1}^8 c_k \omega_k}, \quad (10)$$

Evaluation of the sum (10) gives:

$$\begin{aligned} H_{(2)} &= 2 \left(H_{(2)}^{(0,0,0,1,0,-1,0,0)} + H_{(2)}^{(0,0,0,-1,0,1,0,0)} + H_{(2)}^{(0,0,0,0,1,0,0,-1)} + H_{(2)}^{(0,0,0,0,-1,0,0,1)} \right) \\ &= - \left(\frac{[H_{(2)}^{(0,0,0,0,0,-1,0,0)}, H_{(2)}^{(0,0,0,1,0,0,0,0)}]}{\omega_p + \omega} + \frac{[H_{(2)}^{(0,0,0,0,0,1,0,0)}, H_{(2)}^{(0,0,0,-1,0,0,0,0)}]}{-(\omega_p + \omega)} \right. \\ &\quad \left. + \frac{[H_{(2)}^{(0,0,0,0,0,0,0,-1)}, H_{(2)}^{(0,0,0,0,1,0,0,0)}]}{\omega_p - \omega} + \frac{[H_{(2)}^{(0,0,0,0,0,0,0,1)}, H_{(2)}^{(0,0,0,0,-1,0,0,0)}]}{-(\omega_p - \omega)} \right) \\ &= -\frac{\Omega_s \Omega_d}{4(\omega_p + \omega)} [\hat{a}^2, \hat{a}^\dagger] + \frac{\Omega_s \Omega_d}{4(\omega_p + \omega)} [\hat{a}^{\dagger 2}, \hat{a}] - \frac{\Omega_s \Omega_d}{4(\omega_p - \omega)} [2\hat{a}^\dagger \hat{a}, \hat{a}] + \frac{\Omega_s \Omega_d}{4(\omega_p - \omega)} [2\hat{a}^\dagger \hat{a}, \hat{a}^\dagger] \\ &= \frac{\omega \Omega_s \Omega_d}{\omega_p^2 - \omega^2} (\hat{a}^\dagger + \hat{a}), \end{aligned} \quad (11)$$

which is consistent with the result obtained from the Magnus expansion [11].

The QHO squeezing operator $\hat{S}(r)$, generated via parametric excitation, can also be analyzed using Floquet theory. Similarly, application of a single quadrupole tone at frequency ω_p results in a Hamiltonian:

$$\frac{\hat{H}}{\hbar} = \omega \hat{a}^\dagger \hat{a} + \Omega_q (\hat{a} + \hat{a}^\dagger)^2 \cos(\omega_p t), \quad (12)$$

where $\omega_p = 2\omega/K + \delta$ and $\Omega_q = eV_q \eta^2 / \hbar$.

Transforming into the interaction picture with respect to $\omega \hat{a}^\dagger \hat{a}$, the Hamiltonian (12) becomes:

$$\begin{aligned} \frac{\hat{H}_I}{\hbar} &= \frac{\Omega_q}{2} \left(\hat{a}^2 e^{-i(2\omega + \omega_p)t} + \hat{a}^{\dagger 2} e^{i(2\omega + \omega_p)t} \right) \\ &\quad + \frac{\Omega_q}{2} \left(\hat{a}^2 e^{i(\omega_p - 2\omega)t} + \hat{a}^{\dagger 2} e^{-i(\omega_p - 2\omega)t} \right) \\ &\quad + \frac{\Omega_q}{2} (2\hat{a}^\dagger \hat{a} + 1) (e^{i\omega_p t} + e^{-i\omega_p t}) \end{aligned} \quad (13)$$

The Hamiltonian can be treated as a sum of three Hermitian components, each composed of a factor Ω_i , ladder operators, and a time dependence $e^{\pm i\omega_i t}$, where $\{\Omega_1 = \Omega_q, \omega_1 = (2/K + 2)\omega\}$, $\{\Omega_2 = \Omega_q, \omega_2 = (2/K - 2)\omega\}$ and $\{\Omega_3 = \Omega_q, \omega_3 = 2\omega/K\}$.

Using Eqs. (A16) and (A17) in Ref. [26], the K^{th} -order term of the Hamiltonian can be approximately expressed as $\hat{H} = \Omega^K / (\omega/2)^{K-1} (\hat{a}^2 + \hat{a}^{\dagger 2})$, creating a squeezing operator $\hat{S}(r)$ where $r \propto \Omega^K / (\omega/2)^{K-1}$.

Appendix B: QuTiP Simulations

Simulations were conducted in QuTiP by time-evolving the initial state under the influence of the subharmonic excitation Hamiltonian (4) via the time-dependent Schrödinger equation. Constituent data points in Figs. 5(a-b) were obtained by simulating the system at different detunings δ to extract a lineshape, which was fitted using a sinc-squared lineshape to extract the maximum mean phonon number, linewidth, and center frequency. This procedure was repeated at different values of the target variable to extract the dependence on the target variable. The subharmonic excitation Hamiltonian was pulse-shaped in simulation using a tapered-cosine window with $100\mu\text{s}$ rise and fall times and a total length of 1.2ms. The basis size was varied for each data point to reduce simulation overheads, though confirmed to be sufficiently large to contain all simulation dynamics. The Fock state populations and Wigner functions were extracted for each simulation to confirm that a coherent state was produced.

The mean phonon number scales as V_d^2 for all orders of subharmonic excitation, where V_d is the dipole voltage, indicating an overall linear dependence of the displacement on V_d , in agreement with the theoretical analysis and the empirical formulae (3), (9). Simulations instead varying the quadrupole voltages V_s, V_q show that the resultant phonon number scales as $(V_s V_q)^{2(K-1)}$, indicating that the displacement scales as $K-1$, again in agreement with the theoretical analysis and the empirical formula (9).

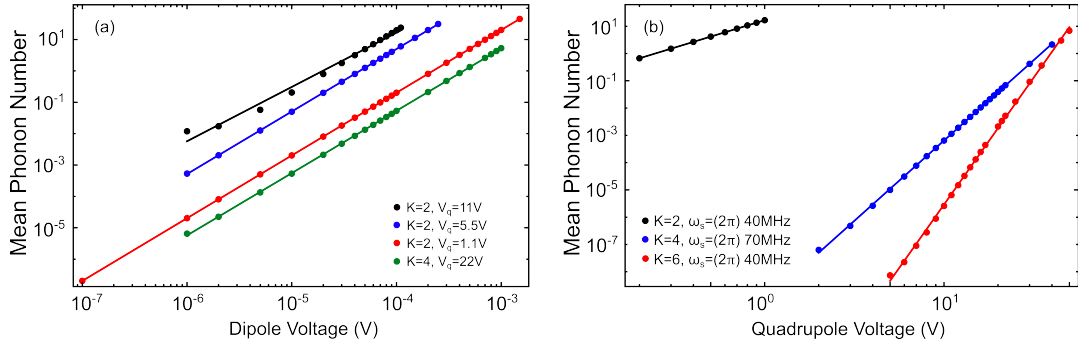


FIG. 5. (a, b) Dependence of the subharmonic excitation on the applied dipole voltage V_d and the applied quadrupole voltages V_s, V_q , respectively. Results are simulated using a $\omega = 1$ MHz secular frequency. A linear model $y = mx + b$ is fitted to the log-log transform of the results to extract the power-law dependence at each subharmonic order. (a) Simulated results at all subharmonic orders exhibit an approximately quadratic dependence of mean phonon number on dipole voltage V_d , equivalent to a linear dependence of displacement on V_d . (b) Simulated results exhibit a power-law scaling of the mean phonon number on V_s, V_q that agrees well with the predicted scaling of $2(K-1)$.

Appendix C: The Standard Quantum Limit (SQL) - Frequency Sensing

The derivation of the SQL for frequency sensing with the QVSA technique is thoroughly presented in [11]. The key distinction between the QVSA technique and the $K = 2$ subharmonic excitation lies in the number of probe tones: the QVSA applies two probe tones detuned from the signal tone at $\pm\omega_{r/z}$, while the $K = 2$ subharmonic excitation applies only a single tone detuned by $\omega_{r/z}$. Thus, the relation between excited phonon and probe tone detuning for the $K = 2$ subharmonic excitation is instead:

$$\langle n \rangle = |\tilde{a}|^2 \frac{\sin^2(\delta\tau/2)}{(\delta\tau/2)^2}, \quad (14)$$

where δ is the detuning of the probe tone and τ is the interrogation time.

As a result, the resolution of the $K=2$ subharmonic excitation is a factor of 2 lower compared to the QVSA measurement. The SQL for frequency sensing is thus:

$$\Delta\delta \approx 2\pi \frac{0.418}{|\tilde{a}|\tau\sqrt{N}} \quad (15)$$

where $|\tilde{a}|$ is the displacement, t is the interrogation time, and N is the number of experiments.

Appendix D: Wideband Sensing with Subharmonic Excitation

To confirm the wide frequency operation of our protocol, we characterized the $K=6$ subharmonic resonance at three different signal frequencies $\omega_s/2\pi = 70, 80$ and 200 MHz (Fig. 6). Traces are normalized by maximum excitation and exhibit highly overlapping lineshapes, making our protocol uniquely suited to the challenges of wideband quantum sensing.

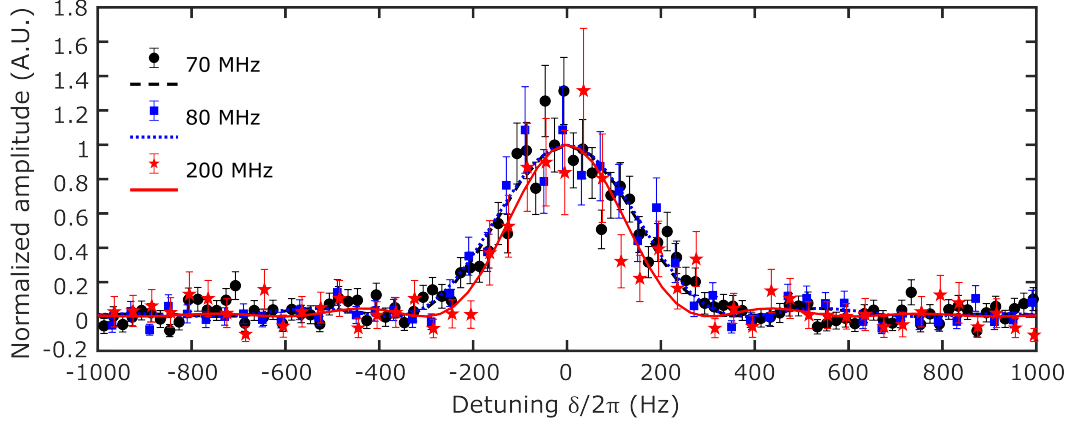


FIG. 6. $K=6$ subharmonic excitation at different signal frequencies ($\omega_s/2\pi = 70, 80$ and 200 MHz). Lines are fits to the data using a sinc-squared profile. All data are normalized by the peak amplitudes of their fit. The interrogation time is fixed at $\tau = 1.2$ ms. Error bars represent one standard error.

Appendix E: The Minimum Frequency Uncertainty of an 80 MHz Signal Tone

To achieve a state of art frequency resolution for an 80 MHz signal tone, we excited the $K = 12$ subharmonic resonance on the axial mode with an interrogation time up to $\tau = 5$ ms, as illustrated in the inset of Fig. 7. The Allan deviation was determined by measuring two points at the FWHM of the motional spectrum. A minimum frequency resolution of $\delta\omega_s/2\pi = 0.56(32)$ Hz after $N = 9600$ experiments. The motional coherence time for the axial mode is 20 ms. The primary limitation on the achievable minimum frequency resolution is the damage threshold of trap electronics (5 Watts). Measurements at other values of K at $\tau = 5$ ms were not pursued to avoid risking damage to the electronic hardware. Upgrades to system electronics would allow excitation of subharmonic orders beyond $K = 12$, improving the minimum resolution by a factor of at least $> 4\times$.

Appendix F: Sensitivity of Phonon Readout

A common method for determining the mean phonon number $\langle n \rangle$ of different quantum states involves measuring the excitation probability (P_r) after a pulse applied for $t = \pi/\Omega_{01}$ the red motional sideband of the $|^2S_{\frac{1}{2}}, m_J = -\frac{1}{2}\rangle \Rightarrow |^2D_{\frac{5}{2}}, m_J = -\frac{5}{2}\rangle$ qubit transition, where Ω_{01} is the Rabi frequency on the blue motional sideband on the same transition.

The Fisher information for this phonon readout technique is $F(n) = \sum \frac{1}{P_r} \left(\frac{\partial P_r}{\partial n} \right)^2 = \frac{1}{P_r(1-P_r)} \left(\frac{\partial P_r}{\partial n} \right)^2$. From Fig. 8, $\left(\frac{\partial P_r}{\partial n} \right)^2$ is consistently larger for coherent states than squeezed states for all values of $\langle n \rangle$, indicating that coherent states offer a higher Fisher information and thus greater detection sensitivity, making them more suitable for precision measurement.

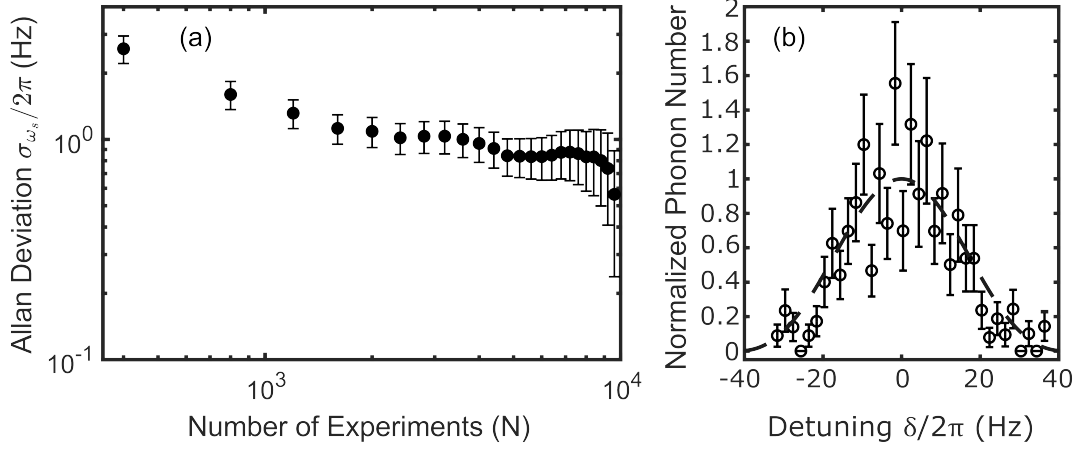


FIG. 7. High resolution scan of an 80 MHz probe tone using the $K = 12$ subharmonic resonance on the axial mode. (a) An overlapped Allan deviation yields a minimum frequency uncertainty $\delta\omega_s/2\pi = 0.56(32)$ Hz at $N = 9600$. The interrogation time is fixed at $\tau = 5$ ms. Each individual experiment takes 22 ms and is comprised of cooling pulses, the subharmonic excitation sequence, and state detection. (b) Motional excitation spectrum generated by scanning the frequency of the probe tone. Error bars represent one standard error.

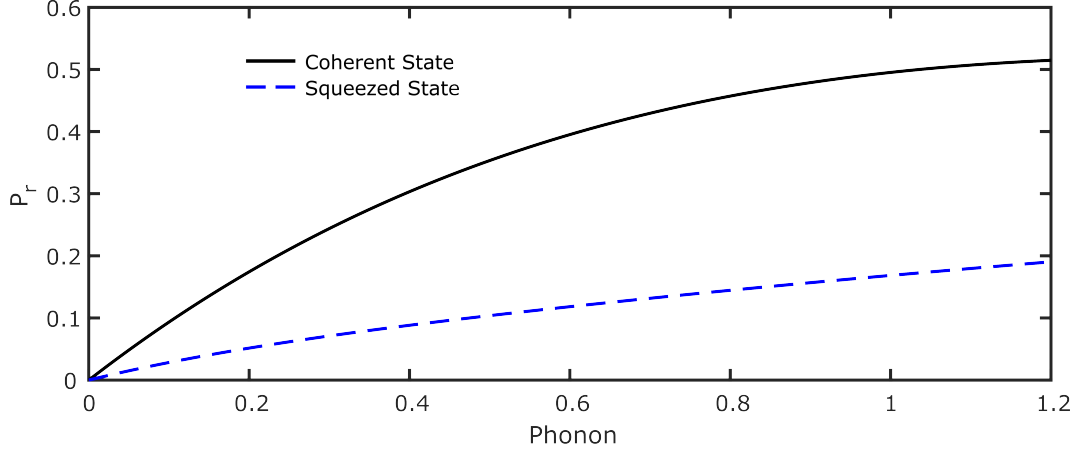


FIG. 8. The relation between population probability in dark clock state state $|^2D_{\frac{5}{2}}\rangle$ and phonon number for different motional states. The population is measured after applying red sideband Rabi oscillation for interrogation time $\tau = \pi/\Omega_{01}$, where Ω_{01} is the Rabi frequency for the $|^2S_{\frac{1}{2}}, m_J = -\frac{1}{2}, n = 0\rangle$ to $|^2D_{\frac{5}{2}}, m_J = -\frac{5}{2}, n = 1\rangle$ transition.